

Poly(oligo(ethylene glycol) methyl ether methacrylate) Brushes on High- κ Metal Oxide Dielectric Surfaces for Bioelectrical Environments

Daniel Y. Joh,[†] Felicia McGuire,[‡] Roozbeh Abedini-Nassab,[§] Joseph B. Andrews,[‡] Rohan K. Achar,[†] Zackary Zimmers,[†] Darush Mozhdehi,[†] Rebecca Blair,[†] Faris Albarghouthi,[†] William Oles,[†] Jacob Richter,[†] Cassio M. Fontes,[†] Angus M. Hucknall,[†] Benjamin B. Yellen,[§] Aaron D. Franklin,^{‡,||} and Ashutosh Chilkoti^{*,†}

[†]Department of Biomedical Engineering, Pratt School of Engineering, Duke University, Durham, North Carolina 27708, United States

[‡]Department of Electrical and Computer Engineering, Pratt School of Engineering, Duke University, Durham, North Carolina 27708, United States

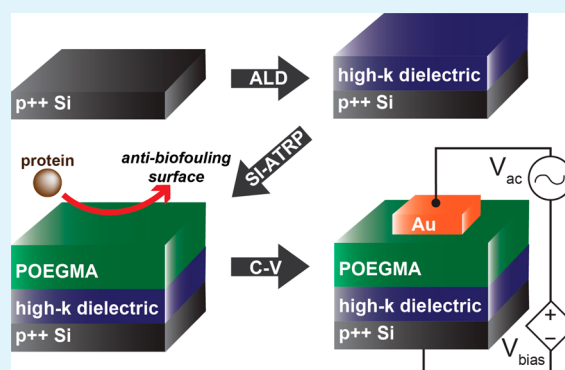
[§]Department of Mechanical Engineering and Materials Science, Pratt School of Engineering, Duke University, Durham, North Carolina 27708, United States

^{||}Department of Chemistry, Duke University, Durham, North Carolina 27708, United States

Supporting Information

ABSTRACT: Advances in electronics and life sciences have generated interest in “lab-on-a-chip” systems utilizing complementary metal oxide semiconductor (CMOS) circuitry for low-power, portable, and cost-effective biosensing platforms. Here, we present a simple and reliable approach for coating “high- κ ” metal oxide dielectric materials with “non-fouling” (protein- and cell-resistant) poly(oligo(ethylene glycol) methyl ether methacrylate) (POEGMA) polymer brushes as biointerfacial coatings to improve their relevance for biosensing applications utilizing advanced electronic components. By using a surface-initiated “grafting from” strategy, POEGMA films were reliably grown on each material, as confirmed by ellipsometric measurements and X-ray photoelectron spectroscopy (XPS) analysis. The electrical behavior of these POEGMA films was also studied to determine the potential impact on surrounding electronic devices, yielding information on relative permittivity and breakdown field for POEGMA in both dry and hydrated states. We show that the incorporation of POEGMA coatings significantly reduced levels of nonspecific protein adsorption compared to uncoated high- κ dielectric oxide surfaces as shown by protein resistance assays. These attributes, combined with the robust dielectric properties of POEGMA brushes on high- κ surfaces open the way to incorporate this protein and cell resistant polymer interface into CMOS devices for biomolecular detection in a complex liquid milieu.

KEYWORDS: POEGMA, metal oxide dielectric, capacitance–voltage, breakdown, nonfouling, biointerface, polymer brush, permittivity



1. INTRODUCTION

The growing emphasis in personalized medicine and targeted therapies has led to much interest in high-performance biosensors, which detect the presence of target analytes in biological systems.¹ Progress in both semiconductor technology and the life sciences have created new possibilities for “lab-on-a-chip” applications based on metal oxide semiconductor (CMOS) circuitry.^{2–5} Notably, advanced CMOS technology employing high-permittivity (“high- κ ”) gate dielectric materials are actively being pursued to satisfy continued scaling and performance demands of the industry beyond the 45 nm technology node (for an excellent synopsis, see review by Robertson and Wallace⁶). These high-performance platforms, when integrated as “lab-on-a-chip” biosensors, may ultimately

enable high-throughput, miniaturized, portable, cost-effective, and low-power devices that are compatible with automated and/or potentially disposable point-of-care platforms.^{7,8} A major challenge to developing CMOS-based biosensing devices is that electronic circuits are designed to function in a dry state, while most biological measurements occur in complex hydrated environments such as blood, serum, urine, and saliva. This dichotomy provides the motivation to incorporate “biointerfacial” materials that permit operation of electronic circuitry within a physiological medium.

Received: December 9, 2016

Accepted: January 24, 2017

Published: January 24, 2017

For a biointerfacial material to be successfully implemented in a biosensor, it must not only be able to immobilize biorecognition elements (e.g., enzymes, antibodies, oligonucleotides, etc.) that target analytes of interest, but also prevent denaturation of these reagents to preserve their biomolecular interactions and thus the fidelity of the sensing signal produced by the device. Another complicating factor is that the overall performance of the device can be impaired by nonspecific binding (NSB) events, especially when exposed to complex biological milieu (e.g., blood, urine, saliva).⁹ NSB can result in false-positive signals and also lowers signal-to-noise ratios (SNR), and this limitation has already been identified as a critical issue in electronic biosensing systems reported to date.^{10–13} Thus, choosing a biointerfacial material that also exhibits “non-fouling” (protein- and cell-resistant) properties while maintaining high SNRs and preserving specific binding between biorecognition elements and target analytes is highly desirable.

One possible strategy to impart these biointerfacial properties to CMOS structures is by using a polymer brush as the interface,^{4,14–24} given their many tunable properties such as main chain length, side chain length, and surface density^{25–27} and ability to be patterned with standard micro-fabrication techniques.^{28,29} In particular, poly(oligo(ethylene glycol) methyl ether methacrylate) (POEGMA) polymer brushes are well-suited for modifying the surface properties of biosensor devices in a manner that satisfies all the criteria described above. POEGMA, a derivative of the widely used polymer poly(ethylene glycol) (PEG), exhibits superior nonfouling properties compared to linear PEG because its 3-dimensional “bottle-brush” structure allows higher densities of oligo(ethylene glycol) functional groups to be presented at the solid/water interface.^{23,30} We have previously shown that POEGMA can be uniformly grown by surface-initiated atom transfer radical polymerization (SI-ATRP) on gold,²⁵ glass^{29,31,32} and plastics,²⁹ and easily patterned with various lithographic approaches with excellent spatial resolution.^{23,29,33–35} Our previous work has also shown that antibodies—the prototypical capture reagents for immunoassays—can be inkjet-printed into a POEGMA brush without the need for any covalent coupling and that the printed antibodies are stabilized by the brush such that they remain active for months without the need stored under hydrated conditions or refrigeration.^{32,36} Finally, POEGMA brushes show excellent nonfouling behavior, even in complex biological milieu such as whole blood and serum, which translates to high SNRs when integrated into sensing systems.^{21,26,27,32,37}

Here, we report on the fabrication of nonfouling biointerfacial coatings with POEGMA on high- κ dielectric metal oxides. We show that nanoscale POEGMA films are reliably grown from high- κ metal oxide surfaces using a “grafting from” approach, as confirmed by ellipsometric measurements and X-ray photoelectron spectroscopy (XPS) analysis. We also characterize the response of POEGMA films to applied electric fields to determine their dielectric and breakdown properties, and finally show that these coatings significantly reduce biomolecular noise from NSB on dielectric metal oxide surfaces. We believe that these results will help pave the way to integrate high- κ metal gate (HKMG) dielectric technology into electronic biosensing systems.

2. EXPERIMENTAL SECTION

2.1. Atomic Layer Deposition. Atomic layer deposition (ALD) was employed to deposit conformal thin films with atomic-scale precision. Metal precursors and oxygen sources are sequentially introduced into the chamber, leading to deposition of dielectric materials with monolayer-by-monolayer control. A detailed description of ALD can be found elsewhere.³⁸ In this study, we used the Savannah S200 ALD system by Ultratech/CambridgeNanotech (Waltham, MA). Prior to ALD, silicon wafers were thoroughly cleaned with piranha (3:1 sulfuric acid: 30% hydrogen peroxide), rinsed copiously with deionized water and then isopropyl alcohol, and then gently blown dry with N₂ gas. The operating temperature for ALD was 150 °C. For all runs, the Savannah S200 ALD system was first allowed to stabilize for at least 10 min prior to performing coating steps. The specific system settings and recipe used for each metal oxide dielectric material are summarized in Table S1 in the Supporting Information Section.

2.2. SI-ATRP of POEGMA on Oxide Dielectrics. **2.2.1. Surface Functionalization with APTES and Installation of Bromide Initiator.** Unless otherwise stated, steps were performed under ambient conditions. The oxide samples described above were immersed in a 10% solution of 3-aminopropyltriethoxysilane (APTES) (Gelest, Inc.; Morrisville, PA) in ethanol overnight, and subsequently rinsed with fresh ethanol and then with deionized water. Chips were spun dry at 150 rcf for 5 min and then cured in an oven at 120 °C for 2 h. Next, the chips were cooled to room temperature then placed in a dichloromethane solution containing 1% α -bromoisobutryl bromide (BIB) and 1% triethylamine (TEA) (Sigma-Aldrich; St. Louis, MO) for 45 min, followed by rinsing in fresh dichloromethane, then ethanol, and then in deionized water. The chips were spun dry 150 rcf for 5 min and then stored under ambient conditions.

2.2.2. Preparation of Polymerization Solution. A solution composed of 350 mL deionized water, 25 mg copper(II) bromide, 50 μ L of 1,1,4,7,10,10-Hexamethyltriethylenetetramine (HMTETA), and 75 g of inhibitor-free poly(ethylene glycol) methyl ether methacrylate ($M_n \approx 300$) were degassed by He-sparging for 3 h.

2.2.3. Surface-Initiated Atom-Transfer Radical Polymerization. Under an Ar environment, 800 mg of sodium ascorbate was added to the polymerization solution described above and gently stirred for 1 min, at which point the solution changed color from blue to violet. The chips were then placed in this solution for polymerization (without stirring). After allowing polymerization to proceed for the desired time points, chips were rinsed three times with deionized water, then centrifuged at 150 rcf for 6 min and allowed to dry under ambient conditions. The thickness of POEGMA brush was determined by reflective-mode ellipsometry, as described below.

2.3. SI-ATRP of POEGMA on Gold. Si chips were coated with 10 nm of Au using electron-beam evaporation (Kurt J. Lesker Company, Jefferson Hills PA). Au-coated chips were immersed in a 10% solution of Bis[2-(2-bromoisobutyryloxy)undecyl] disulfide (Sigma-Aldrich; St. Louis, MO) in anhydrous ethanol overnight, and subsequently rinsed with ethanol and then three times with deionized water. The chips were centrifuged and then allowed to dry in ambient conditions. Subsequently, steps B and C were performed as described above to grow POEGMA brushes.

2.4. Reflective Mode Ellipsometry. The thickness of thin films were measured using an M-88 spectroscopic ellipsometer (J.A. Woollam Co) at angles of 65°, 70°, and 75° at wavelengths of 400 to 800 nm. The thickness of the layers underlying the POEGMA films were each determined experimentally based on the optical constants of these materials provided in the instrument software, and were then used to build a model. The POEGMA film thicknesses were then determined using a Cauchy layer algorithm. For all ellipsometric measurements, we chose the thickness for which the mean standard error between the predicted response from the model and the experimental response from the sample reached a global minimum. Only those data which yielded good fitting results (mean square error ≤ 0.9) were used to determine film thicknesses.

2.5. X-ray Photoelectron Spectroscopy. All XPS experiments were performed on an AXIS Ultra photoelectron spectrometer (Kratos

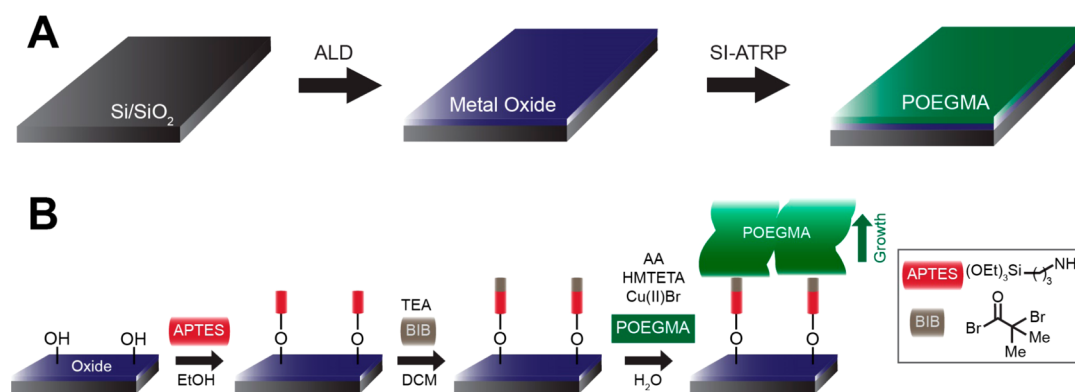


Figure 1. POEGMA brush growth from dielectric oxide materials by surface-initiated atom transfer radical polymerization. (A) Representative workflow. Si chips with 20 nm thermal oxide underwent ALD of metal oxides (TiO_2 , ZrO_2 , Al_2O_3). POEGMA brushes were then grown from oxide surfaces by SI-ATRP. (B) Stepwise illustration of POEGMA growth strategy. APTES attachment to oxide surfaces enables functionalization with ATRP initiator (BIB), enabling POEGMA brushes to be “grafted from” substrate surfaces. Legend: molecular structures of APTES and BIB initiator (α -bromoisobutryl bromide). Abbreviations: EtOH = ethanol, DCM = dichloromethane, TEA = triethylamine, SA = sodium ascorbate, HMTETA = 1,1,4,7,10,10-hexamethyltriethylenetetramine.

Analytical, NY) operating at 15 kV and 10 mA using monochromatic $\text{K}\alpha 1$ X-rays. The X-ray spot size was 400 μm (full-width at half-maximum). Survey scans and high-resolution core-level spectra were recorded with the following pass energy, energy step, dwell time, and number of sweeps: survey spectra -160 eV, 1 eV, 200 ms, and 10 sweeps; high-resolution core-level spectra -20 eV, 0.1 eV, 269.7 ms, and 20 sweeps. The operating pressure of the instrument was $\sim 1 \times 10^{-8}$ Torr. The spectral data were analyzed using CasaXPS software.

2.6. Electrical Characterization of POEGMA. Parallel plate capacitors with an area of $2 \times 2 \text{ mm}^2$ were fabricated by growing POEGMA on p^+ Si wafers with a 10.4 nm overlayer of thermal SiO_2 , and then utilizing a shadow mask to deposit 5 nm Ti (adhesion layer) and 30 nm Au top contacts with a custom-built Kurt J. Lesker electron-beam evaporator system. The capacitance–voltage (C – V) measurements were performed using an Agilent (Keysight Technologies) B1500A Semiconductor Parameter Analyzer connected via triaxial cables to a Lakeshore CRX 6.5K cryogenic probe station, where one probe was placed on the top contact and a second probe was connected to a back-gated chuck upon which the sample was placed. C – V measurements were obtained at frequencies of 1 MHz, 100 kHz, and 10 kHz from multiple capacitors on the same chip. In order to compare C – V measurements for hydrated POEGMA versus dried POEGMA, characterization was first performed on a dry sample, and then the chip was placed in 1X PBS buffer for 5 min to hydrate the POEGMA. The back of the sample was then dried using a gentle stream of nitrogen gas, and the C – V measurement process was repeated. Finally, the hydrated sample was dried under overnight under vacuum, and a final C – V measurement was obtained and the permittivity extracted once again. For further characterization, a breakdown of the POEGMA was obtained by growing POEGMA on a patterned gold electrode and then depositing a 5 nm Ti adhesion layer and a 30 nm Au top contact using a shadow mask, and the breakdown voltage was determined by measuring current density versus electric field.

2.7. Surface Adsorption of Proteins. SiO_2 , TiO_2 , ZrO_2 , and Al_2O_3 surfaces with and without POEGMA coatings were exposed to a 1 mg/mL solution of Cy5-BSA in 1X PBS buffer for 4 h. Substrates were then rinsed with a PBS solution containing 0.1% Tween20 to remove any unbound proteins, centrifuged at 4800 rpm for 15 s to wick away excess liquid, then allowed to dry under ambient conditions. Fluorescence imaging of all samples was performed using an Axon Genepix 4400 tabletop scanner (Molecular Devices, LLC; Sunnyvale, CA) under identical imaging conditions with an exciting wavelength of 635 nm; fluorescence intensity analysis was performed using ImageJ Fiji.³⁹

3. RESULTS AND DISCUSSION

The substrate materials used in this study were chosen for their relevance to the semiconductor and electronics industry, and included three high-permittivity (“high- κ ”) metal oxide dielectrics: TiO_2 ($\kappa \approx 80$), ZrO_2 ($\kappa \approx 23$), and Al_2O_3 ($\kappa \approx 10$). For comparison, we also included studies on thermally deposited SiO_2 ($\kappa \approx 3.9$) on Si, given the existing body of work on growing POEGMA from glass and SiO_2/Si substrates.^{23,29,31,32} The high- κ metal oxide dielectrics were fabricated as 10 nm thick layers using atomic layer deposition (ALD) onto Si wafers. The layer-by-layer control offered by ALD allows ultrathin films of just a few nanometers to be fabricated in a highly reproducible and precise manner,³⁸ and is widely used in semiconductor manufacturing, especially for emerging electronic architectures with spatial demands below the 100 nm regime. Hence, these dielectric layers offer the most relevant surface for establishing a biointerfacial film that will serve to both passivate the underlying CMOS structures from liquid biological environments so that it can be used in conjunction with the biointerfacial film for biomolecular detection.

A summary of the synthesis route for the biointerfacial POEGMA brushes fabricated on metal oxide dielectric surfaces is shown in Figure 1. The approach relies on surface-initiated atom transfer radical polymerization (SI-ATRP) to grow POEGMA from oxide surfaces that were prefunctionalized with an ATRP initiator,^{15,28,32} using a subtype of SI-ATRP that utilizes an aqueous environment and activators regenerated by electron transfer (ARGET).⁴⁰ This approach was used as it produces films with tunable thickness, requires only small amounts of transition metal catalyst, uses an environmentally friendly reducing agent (sodium ascorbate) that drastically reduces the requirements for tedious deoxygenation procedures, and is performed in water (rather than organic solvent) as the reaction medium. In combination, these features are attractive for reducing production costs and processing complications, especially when producing POEGMA films at scale.

The growth behavior of ARGET SI-ATRP-based was investigated by reflective mode spectroscopic ellipsometry in air. Figure 2A shows the growth of POEGMA on TiO_2 , ZrO_2 , and Al_2O_3 surfaces, and on SiO_2 as a comparison. The thickness

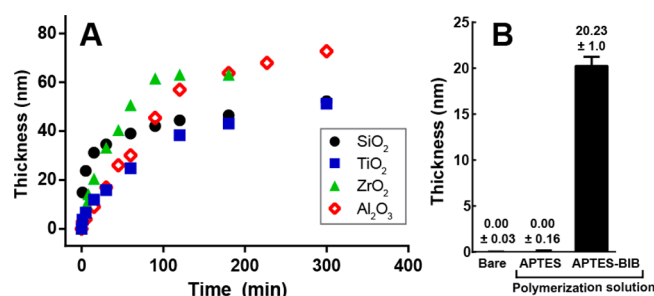


Figure 2. Growth behavior of POEGMA brushes grown by SI-ATRP on oxide dielectrics. (A) POEGMA brush growth was measured by reflective mode ellipsometry at the indicated time points for Si/SiO₂, TiO₂, ZrO₂, and Al₂O₃. (B) Control experiment showing that surface-immobilized bromide initiator is required for POEGMA brush growth. Si/SiO₂ chips coated with APTES alone and then placed in polymerization solution do not show any appreciable polymer brush growth after 60 min, while chips with bromide initiator installed (APTES+BIB) show 20 nm brushes.

of the POEGMA brush progressively increases over time in a controlled manner, reaching thicknesses of approximately 50–70 nm under these experimental conditions. The data show consistent film thicknesses between substrate replicates per time point, and the observed minor differences in final film thickness for each POEGMA brush layer is likely due to small variances in reaction conditions between batches (e.g., residual oxygen leading to premature chain termination).⁴¹ Importantly, the 50–70 nm brush thicknesses are well above the minimum values for which POEGMA surfaces exhibit nonfouling behavior: brushes thicker than ~9.5 nm were previously shown to be exceptionally resistant to the adventitious adsorption of “sticky” proteins such as fibronectin, in addition to components of complex biological media such as undiluted serum.^{29,31,42} Thus, these methods lead to POEGMA brushes that reach adequate thicknesses for use as nonfouling biointerfacial layers on high- κ metal oxide dielectrics. As a control experiment, we compared the growth of POEGMA on SiO₂ substrates coated with APTES only versus substrates coated with APTES plus bromide initiator (APTES-BIB). The

data in Figure 2B show that Si/SiO₂ chips coated with APTES alone and then placed in polymerization solution do not show any appreciable polymer brush growth after 60 min, while chips with bromide initiator installed (APTES+BIB) grew 20 nm brushes. These results unequivocally confirm that POEGMA only grows from a surface as a result of polymerization originating from the ATRP initiator that is chemically attached to the substrate surface.

To characterize the POEGMA films in greater detail, we used X-ray photoelectron spectroscopy (XPS) to analyze the molecular composition of the substrate, the initiator functionalized surface, and the POEGMA overlayers (Figure 3). The dashed traces in Figure 3 show survey spectra of SiO₂, TiO₂, ZrO₂, and Al₂O₃ surfaces after surface functionalization with APTES-BIB, but prior to polymerization. Each of the survey spectra exhibits the characteristic peaks associated with each oxide dielectric.^{43–45} In addition, a small peak at ~399 eV matching an N 1s photoelectron peak is also observed, which corresponds to the nitrogen moieties from APTES immobilized on the surface (except in the case of ZrO₂, where this peak is obscured by the spectral contributions from the metal oxide). The bromide peaks associated with the ATRP initiator were unresolved in our survey spectra; these findings are consistent with previously reported XPS studies on electrochemically assisted growth of TiO₂ films functionalized with APTES-BIB.²⁸

The solid traces in Figure 3 show survey scan spectra of substrates having thick (greater than 25 nm) overlying POEGMA films after SI-ATRP. These film thicknesses are greater than the sampling depth of XPS (which is typically up to ~10 nm for Al K α radiation depending upon the specific core level photoelectrons),⁴⁶ and thus the vast majority of detected photoelectrons are expected to originate from the POEGMA layer. For each POEGMA-coated oxide substrate, the survey scan spectra clearly demonstrate significant changes in elemental composition compared to substrates before polymerization. The spectral peaks associated with the metal oxide dielectrics in Figure 3 are virtually absent, and the spectra of POEGMA-coated substrates appear practically identical, with

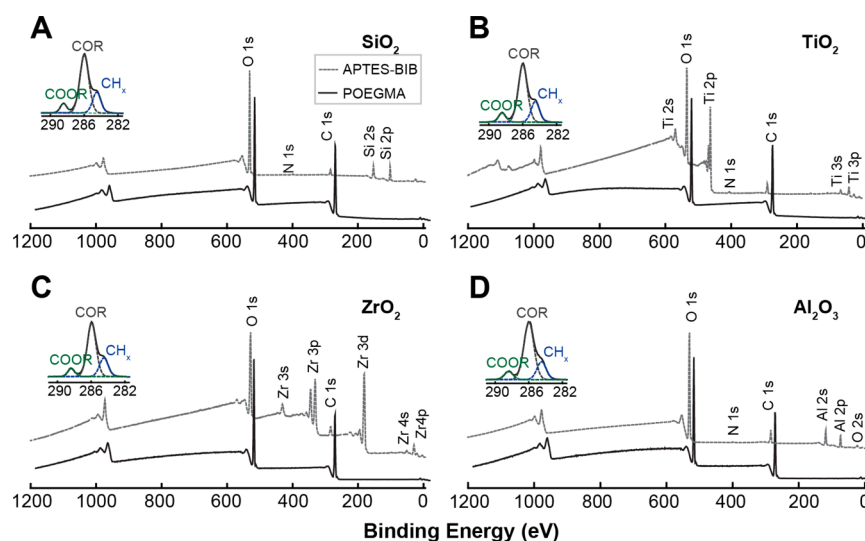


Figure 3. X-ray photoelectron spectra prior to and after SI-ATRP on oxides. (A–D) Dashed traces: survey spectra of initiator-grafted (APTES-BiB) surfaces on Si/SiO₂, TiO₂, ZrO₂, and Al₂O₃. The Br signal was underestimated, preventing its quantification. Solid traces: survey spectra after SI-ATRP of POEGMA brushes. Insets: High resolution C 1s spectra following SI-ATRP, showing peak fits consistent with POEGMA brushes.

Table 1. Atomic Concentrations (%) of Carbon and Oxygen Moieties before (BIB-APTES) and after Polymerization^a

	pre-ATRP (%)			post-ATRP (%)					
	survey			survey			high-res. C 1s		
	C	O	M	C	O	M	CH _x	COR	COOR
SiO ₂	11.5 ± 1.7	53.7 ± 6.7	34.8 ± 8.4	71.3 ± 1.7	28.7 ± 1.7	ND	23.3 ± 1.7	68.1 ± 2.3	8.6 ± 0.6
TiO ₂	24.9 ± 2.0	55.6 ± 1.6	19.5 ± 0.5	72.7 ± 1.3	27.3 ± 1.3	ND	24.2 ± 0.8	67.2 ± 0.7	8.6 ± 0.2
ZrO ₂	30.1 ± 5.8	53.6 ± 5.9	16.3 ± 0.2	72.3 ± 4.0	27.7 ± 4.0	ND	26.9 ± 4.5	65.0 ± 5.6	8.1 ± 1.0
Al ₂ O ₃	23.9 ± 8.2	41.2 ± 9.9	34.9 ± 2.2	71.4 ± 3.4	28.6 ± 3.4	ND	20.2 ± 0.4	71.9 ± 1.5	7.9 ± 1.2

^a“M” stands for metal (Ti, Zr, Al) or metalloid in the case of Si. Values were calculated by curve-fitting to the following peak positions: O 1s (530.6 eV); C 1s (~284.5 eV). CH_x (284.5 eV), COR (286.0 eV), COOR (288.5 eV). Error bars: mean ± s.d. of three separate spectra.

each showing a notably sharp increase in the C 1s (284.5 eV) peak. High-resolution XPS of the C 1s photoemission envelope for each polymer brush-modified substrate (insets, Figure 3) were fit to the three unique carbon moieties of POEGMA: CH_x (284.5 eV), COR (286.7 eV), and COOR (289.1 eV). The molecular composition of each overlayer are summarized in Table 1, all of which are reasonably close to the ~1:3:10 (COOR:CH_x:COR) stoichiometry of POEGMA assuming 4–5 ethylene glycol units in the side-chain of each POEGMA repeat unit. These results are consistent with POEGMA brushes previously grown on gold and glass.^{25,31}

We next studied the response of the POEGMA films under applied electric fields to determine the material's electrical characteristics. Parallel-plate capacitors were fabricated as shown in Figure 4A, by first growing POEGMA on p⁺ doped, low-resistivity Si wafers with a 10.4 nm thick thermally grown SiO₂ overlayer. Top contact electrodes (4 mm² in size) were then formed by evaporating 5 nm Ti and 30 nm Au through a shadow mask in an electron-beam evaporator. Capacitance–voltage (*C*–*V*) measurements from these parallel-plate structures allow us to extract the relative permittivity of POEGMA (ϵ_p). When the device is biased in the strong accumulation regime, the measured capacitance (C_{meas}) is effectively the result of two capacitors in series—one with SiO₂, one with POEGMA.^{47,48} The expression for C_{meas} is described using a parallel-plate model by eq 1, in which *A* is the area, *T*_{ox} and *T*_p are the thickness of the oxide and POEGMA (respectively), and ϵ_{ox} and ϵ_p are the relative permittivity of the oxide and POEGMA (respectively):

$$C_{\text{meas}} = \frac{\epsilon_0 A}{\frac{T_{\text{ox}}}{\epsilon_{\text{ox}}} + \frac{T_p}{\epsilon_p}} \quad (1)$$

A representative *C*–*V* measurement from one of the POEGMA capacitors is given in Figure 4B in which C_{meas} is plotted against bias voltage from a device having a POEGMA film thickness of 24.3 nm. Substituting the strong accumulation capacitance for C_{meas} into eq 1 led to an experimentally determined value for ϵ_p as ~7.07. For biosensing-related applications, devices are exposed to wet environments and thus further *C*–*V* characterization was performed under conditions that more closely mimic the wet environment in which POEGMA films will need to operate. To this end, we submerged the same device from Figure 4B in a 1x PBS buffer for 5 min to hydrate the POEGMA, followed by immediate electrical characterization under ambient conditions.

The response of the POEGMA after hydration with 1X PBS is shown in Figure 4C. The hydrated POEGMA shows a significantly increased relative permittivity ($\epsilon_p = 68.9$) compared to dry POEGMA, approaching a value closer to that of water. This behavior is consistent with the highly

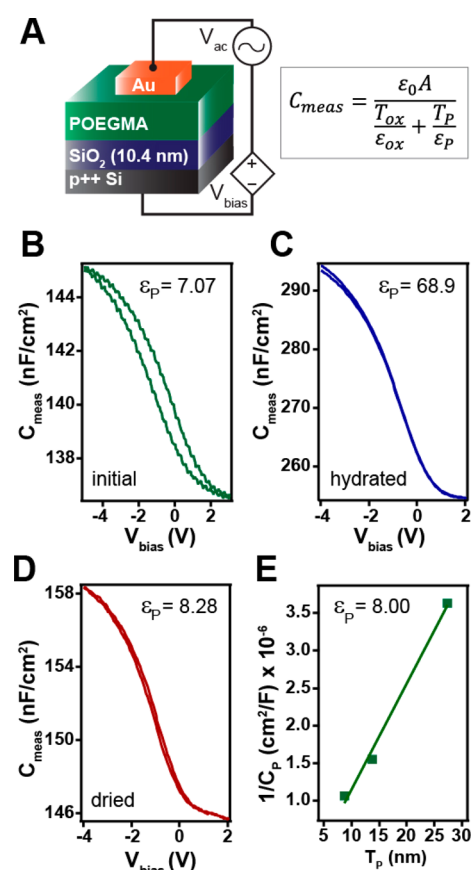


Figure 4. Capacitance–voltage measurements on POEGMA. (A) Schematic of the POEGMA samples used to obtain the capacitance–voltage curves with a detailed expression for the total measured capacitance (C_{meas}) used for determining permittivity. An amplitude of 30 mV was used for V_{AC} . (B–D) Sequence of capacitance–voltage curves from a POEGMA film of 24.3 nm thickness beginning with the initial characteristic (B), followed by the response posthydration of the POEGMA (C), and finally after a drying step to dehydrate (D). (E) Linear fit of the inverse POEGMA capacitance versus thickness used to confirm the extracted permittivity ϵ_p .

hydrophilic nature of POEGMA, leading to water molecules penetrating and residing within the polymer brush by hydrogen bonding interactions.^{49–52} Subsequently, the same sample was dried overnight in a vacuum desiccator to return the POEGMA to a dry state for a final *C*–*V* measurement (Figure 4D). The relative permittivity of the dried POEGMA showed a value ϵ_p of 8.28 that was consistent with the initial measurement (Figure 4B). The slight difference in experimental ϵ_p between the initial and dried samples (Figure 4B,D) may be attributed to the ability for oligoethylene glycol brushes to retain residual

amounts of water after drying.⁵³ This overall behavior is consistent with several studies showing that oligoethylene glycol brushes can reversibly recover their original structure and retain nonfouling characteristics after dehydration cycles,^{53,54} which is particularly relevant to sensing applications requiring repeated use with the same device. To complete the extraction of the permittivity for POEGMA, we grew films of different thicknesses and obtained $C-V$ measurements for each sample. As depicted in eq 2, the capacitance of the POEGMA film (C_p) is inversely related to its thickness (T_p):

$$C_p = \frac{\epsilon_p \epsilon_0 A}{T_p} \quad (2)$$

Figure 4E plots values of $1/C_p$ versus T_p , which yields a linear fit for a more accurate relative permittivity for as-grown POEGMA, calculated to be $\epsilon_p = 8.00$. We note that since the main focus of these experiments was to determine ϵ_p , only devices with SiO_2 dielectric overlayers were required, as the supporting substrate and associated dielectric should have no bearing on the extraction of ϵ_p . There may exist some interfacial effects, but none that we would anticipate hampering the extraction of ϵ_p . Next, to assess the robustness of POEGMA as a dielectric material, the breakdown behavior was characterized, as shown in Figure 5. For these measurements, we used the

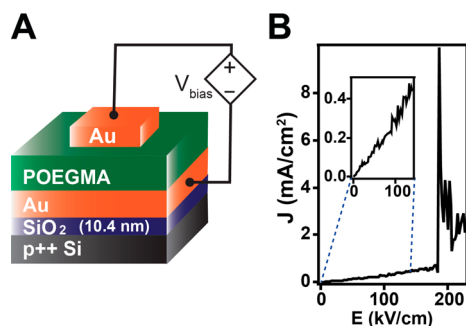


Figure 5. Breakdown characteristics of POEGMA. (A) Schematic of the POEGMA sample used to investigate the breakdown of POEGMA films. A POEGMA film was grown on a patterned gold electrode, followed by depositing a 5 nm Ti adhesion layer and a 30 nm Au top contact (B) Breakdown curve for POEGMA film of 44.2 nm thick, exhibiting a breakdown field of 183.2 kV/cm.

device geometry shown in Figure 5A, by growing POEGMA (44.2 nm) on a patterned gold electrode and subsequently fabricating a gold top contact, then measuring current density under an increasing electric field. The results are shown in Figure 5B, where breakdown is initiated at an applied field of 183.2 kV/cm, confirming that POEGMA functions as a stable dielectric material with a relatively robust breakdown field that is approximately within an order of magnitude of high-quality thermal SiO_2 .

Having characterized the electrical properties of POEGMA coatings, we then sought to investigate the ability for POEGMA films to prevent adventitious adsorption of proteins onto the surface of dielectric oxides. For these protein-resistance studies, we targeted thicknesses of ≥ 9.5 nm of POEGMA in the dry state on all substrates, informed by our previous studies that POEGMA coatings that have an ellipsometrically measured thickness in their dry state above this threshold provide complete protein resistance on a broad range of substrate materials.^{31,42} To this end, dielectric oxide surfaces with and

without POEGMA coatings were incubated with a concentrated solution (1 mg/mL) of Cy5-BSA for 4 h, washed with buffer to remove any unbound proteins, and then imaged with a tabletop fluorescence scanner to detect the presence of residual Cy5-BSA adsorbed onto the surface (Figure 6). The image data

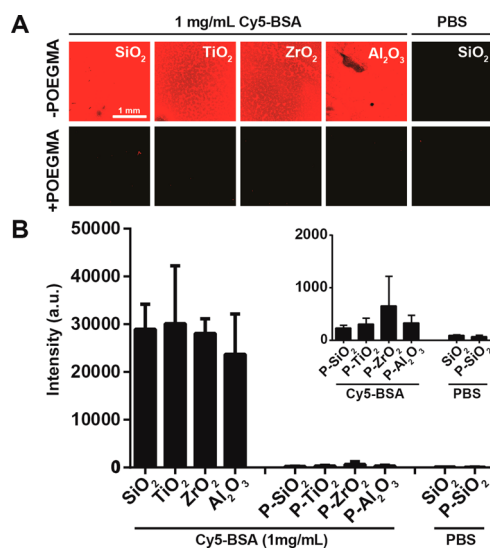


Figure 6. Protein adsorption onto dielectric oxide surfaces with and without POEGMA. (A) Representative fluorescence images of adsorption of Cy5-BSA onto dielectric oxide surfaces with and without POEGMA coatings. Surfaces were incubated for 4 h with 1 mg/mL Cy5-BSA in PBS, washed, and then imaged with a tabletop scanner for residual Cy5 fluorescence. Images of SiO_2 surfaces (with and without POEGMA) treated with PBS vehicle also shown as negative control. (B) Quantitation of fluorescence from residual Cy5-BSA bound to surfaces at the conditions described in (A); data are average \pm s.d. of 3 separate chips. Inset: magnified view of low fluorescence intensity data.

in the top row of Figure 6A show high fluorescence intensity on the surfaces of uncoated substrates compared to PBS vehicle-treated controls, indicating large amounts of nonspecific adsorption of Cy5-BSA. In contrast, substrates that were coated with POEGMA films displayed markedly decreased levels of fluorescent signal, with intensities much closer to those of vehicle controls. Quantitation of the average fluorescence intensities for each dielectric oxide is shown in Figure 6B, which demonstrates that the addition of POEGMA coatings resulted in 40- to 100-fold reduction in the Cy5 signal. Together, these results indicate that coating dielectric oxide surfaces with POEGMA leads to a marked decrease in nonspecific “biomolecular noise”, which is consistent with work done previously by our group and others.^{25–27,31,55–58}

4. CONCLUSIONS

In summary, we have demonstrated that POEGMA coatings can be reliably grown on the surface of high- κ metal oxide dielectric materials using a simple “grafting-from” SI-ATRP strategy. SI-ATRP enables POEGMA films to grow in a controlled manner and reach thicknesses at which POEGMA is known to exhibit highly nonfouling behavior, which will provide a high SNR in biological detection devices by eliminating adventitious adsorption of cells and proteins from the sensor interface. XPS confirmed the fidelity of POEGMA films with respect to their predicted stoichiometry and showed consistent chemical composition of the coatings across each

high- κ growth surface. Next, electrical characterization studies enabled determination of the relative permittivity of POEGMA in both dry and hydrated states, and showed that the POEGMA film behaves as a stable dielectric material with a breakdown field strength that is sufficiently strong for integration in biosensing devices. Finally, we show that interfacial POEGMA films reduced the nonspecific binding of proteins onto dielectric oxide surfaces, suggesting a promising route toward reducing biomolecular noise in CMOS-based biosensors. While the present study focuses on a select number of representative high- κ metal oxide dielectrics (TiO_2 , ZrO_2 , Al_2O_3), the results described herein are applicable by extension to the metal oxides currently favored by the electronics industry such as HfO_2 and Hf-silicate (HfSi_xO_y), and also to Y_2O_3 , La_2O_3 , Sc_2O_3 , Pr_2O_3 , Gd_2O_3 , and Lu_2O_3 that may become relevant as CMOS technology continues to evolve. The results reported herein demonstrate the applicability of POEGMA to bridge electronic transduction with HKMG technology with biological sensing, using a protein-resistant interface. Building off these efforts, future work will involve the development of electronic biosensing platforms incorporating a POEGMA brush interface that are self-contained, label-free, compact, low-power, and suitable for use in a broad range of settings.

■ ASSOCIATED CONTENT

Supporting Information

The Supporting Information is available free of charge on the ACS Publications website at DOI: 10.1021/acsami.6b15836.

Atomic layer deposition conditions (PDF)

■ AUTHOR INFORMATION

Corresponding Author

*Tel: (919) 660-5373. Fax: (919) 660-5409. E-mail: chilkoti@duke.edu (A.C.).

Author Contributions

D.Y.J., F.M., and R.A.N. are colead authors, who participated in experimental design, data collection, data analysis, manuscript drafting, table/figure creation, and manuscript revision. J.A. designed and conducted experiments, analyzed data, and participated in manuscript drafting/revision in matters related to electrical characterization of POEGMA. R.K.A., Z.Z., D.M., R.B., F.A., W.O., J.R., and C.M.F. participated in data collection, data analysis, and manuscript drafting/revision. A.M.H., B.B.Y., and A.D.F. are senior authors involved in study design, oversight, and manuscript drafting/revision. A.C. is the Principal Investigator who directed the studies and drafted/ revised the manuscript. All authors read and approved the final manuscript.

Notes

The authors declare no competing financial interest.

■ ACKNOWLEDGMENTS

The authors gratefully acknowledge generous funding support from the National Heart, Lung, and Blood Institute (1R21HL115410-01) and National Center for Advancing Translational Sciences (UL1TR001117) of the National Institutes of Health. D.Y.J., F.M., and R.A.N. are supported by the Duke University Medical Scientist Training Program (T32GM007171), National Science Foundation Graduate Research Fellowship (Grant No. DGF 1106401) and Lew Siegel Fellowship from the Pratt School of Engineering at Duke University, respectively. The content reflects the views of the

authors and does not necessarily represent the official views of the supporting organizations.

■ REFERENCES

- (1) Phillips, K. A.; Van Bebber, S.; Issa, A. M. Diagnostics and Biomarker development: Priming the Pipeline. *Nat. Rev. Drug Discovery* **2006**, *5* (6), 463–469.
- (2) Pandana, H.; Aschenbach, K. H.; Lenski, D. R.; Fuhrer, M. S.; Khan, J.; Gomez, R. D. A Versatile Biomolecular Charge-Based Sensor Using Oxide-Gated Carbon Nanotube Transistor Arrays. *IEEE Sens. J.* **2008**, *8* (6), 655–660.
- (3) Sarkar, D.; Liu, W.; Xie, X.; Anselmo, A. C.; Mitragotri, S.; Banerjee, K. MoS₂ Field-Effect Transistor for Next-Generation Label-Free Biosensors. *ACS Nano* **2014**, *8* (4), 3992–4003.
- (4) Hess, L. H.; Lyuleeva, A.; Blaschke, B. M.; Sachsenhauser, M.; Seifert, M.; Garrido, J. A.; Deubel, F. Graphene Transistors with Multifunctional Polymer Brushes for Biosensing Applications. *ACS Appl. Mater. Interfaces* **2014**, *6* (12), 9705–9710.
- (5) Estrela, P.; Keighley, S. D.; Li, P.; Migliorato, P. Application of Thin Film Transistors to Label-free Electrical Biosensors. *Proc. IEEE Int. Symp. Ind. Electron.* **2008**, 2034–2039.
- (6) Robertson, J.; Wallace, R. M. High-k Materials and Metal Gates for CMOS Applications. *Mater. Sci. Eng., R* **2015**, *88*, 1–41.
- (7) Arya, S. K.; Wong, C. C.; Jeon, Y. J.; Bansal, T.; Park, M. K. Advances in Complementary-Metal-oxide-Semiconductor-based Integrated Biosensor Arrays. *Chem. Rev.* **2015**, *115* (11), 5116–5158.
- (8) Lei, K.-M.; Mak, P.-I.; Law, M.-K.; Martins, R. P. CMOS Biosensors for In Vitro Diagnosis - Transducing Mechanisms and Applications. *Lab Chip* **2016**, *16* (19), 3664–3681.
- (9) Gosling, J. P. A Decade of Development in Immunoassay Methodology. *Clin. Chem.* **1990**, *36*, 1408–1427.
- (10) Makowski, M. S.; Ivanisevic, A. Molecular Analysis of Blood with Micro-/Nanoscale Field-Effect-Transistor Biosensors. *Small* **2011**, *7* (14), 1863–1875.
- (11) Liu, S.; Guo, X. Carbon Nanomaterials Field-Effect-Transistor-Based Biosensors. *NPG Asia Mater.* **2012**, *4*, e23.
- (12) Estrela, P.; Paul, D.; Song, Q.; Stadler, L. K. J.; Wang, L.; Huq, E.; Davis, J. J.; Ferrigno, P. K.; Migliorato, P. Label-Free Sub-picomolar Protein Detection with Field-Effect Transistors. *Anal. Chem.* **2010**, *82* (9), 3531–3536.
- (13) Rastogi, A.; Nad, S.; Tanaka, M.; Mota, N. D.; Tague, M.; Baird, B. A.; Abruña, H. D.; Ober, C. K. Preventing Nonspecific Adsorption on Polymer Brush Covered Gold Electrodes Using a Modified ATRP Initiator. *Biomacromolecules* **2009**, *10* (10), 2750–2758.
- (14) Krishnamoorthy, M.; Hakobyan, S.; Ramstedt, M.; Gautrot, J. E. Surface-initiated Polymer Brushes in the Biomedical Field: Applications in Membrane Science, Biosensing, Cell Culture, Regenerative Medicine and Antibacterial Coatings. *Chem. Rev.* **2014**, *114* (21), 10976–11026.
- (15) Edmondson, S.; Osborne, V. L.; Huck, W. T. S. Polymer Brushes via Surface-initiated Polymerizations. *Chem. Soc. Rev.* **2004**, *33* (1), 14–22.
- (16) Zhou, F.; Huck, W. T. S. Surface Grafted Polymer Brushes as Ideal Building Blocks for "Smart" Surfaces. *Phys. Chem. Chem. Phys.* **2006**, *8* (33), 3815–3823.
- (17) Jung, D.-H.; Park, I. J.; Choi, Y. K.; Lee, S.-B.; Park, H. S.; Rühle, J. Perfluorinated Polymer Monolayers on Porous Silica for Materials with Super Liquid Repellent Properties. *Langmuir* **2002**, *18* (16), 6133–6139.
- (18) Azzaroni, O.; Moya, S.; Farhan, T.; Brown, A. A.; Huck, W. T. S. Switching the Properties of Polyelectrolyte Brushes via "Hydrophobic Collapse". *Macromolecules* **2005**, *38* (24), 10192–10199.
- (19) Lego, B.; Skene, W. G.; Giasson, S. Swelling Study of Responsive Polyelectrolyte Brushes Grafted from Mica Substrates: Effect of pH, Salt, and Grafting Density. *Macromolecules* **2010**, *43* (9), 4384–4393.
- (20) Chen, L.; Liu, M.; Lin, L.; Zhang, T.; Ma, J.; Song, Y.; Jiang, L. Thermal-responsive Hydrogel Surface: Tunable Wettability and

Adhesion to Oil at the Water/Solid Interface. *Soft Matter* **2010**, *6* (12), 2708–2712.

(21) Lee, B. S.; Chi, Y. S.; Lee, K. B.; Kim, Y. G.; Choi, I. S. Functionalization of Poly(oligo(ethylene glycol) methacrylate) Films on Gold and Si/SiO₂ for Immobilization of Proteins and Cells: SPR and QCM Studies. *Biomacromolecules* **2007**, *8* (12), 3922–3929.

(22) Gautrot, J. E.; Huck, W. T.; Welch, M.; Ramstedt, M. Protein-resistant NTA-functionalized Polymer Brushes for Selective and Stable Immobilization of Histidine-tagged Proteins. *ACS Appl. Mater. Interfaces* **2010**, *2* (1), 193–202.

(23) Hucknall, A.; Rangarajan, S.; Chilkoti, A. In Pursuit of Zero: Polymer Brushes that Resist the Adsorption of Proteins. *Adv. Mater.* **2009**, *21* (23), 2441–2446.

(24) Gautrot, J. E.; Trappmann, B.; Ocegüera-Yanez, F.; Connelly, J.; He, X.; Watt, F. M.; Huck, W. T. Exploiting the Superior Protein Resistance of Polymer Brushes to Control Single Cell Adhesion and Polarisation at the Micron Scale. *Biomaterials* **2010**, *31* (18), 5030–5041.

(25) Ma, H.; Wells, M.; Beebe, T. P.; Chilkoti, A. Surface-Initiated Atom Transfer Radical Polymerization of Oligo(ethylene glycol) Methyl Methacrylate from a Mixed Self-Assembled Monolayer on Gold. *Adv. Funct. Mater.* **2006**, *16* (5), 640–648.

(26) Jin, Z.; Feng, W.; Beisser, K.; Zhu, S.; Sheardown, H.; Brash, J. L. Protein-resistant Polyurethane Prepared by Surface-initiated Atom Transfer Radical Graft Polymerization (ATRGp) of Water-Soluble Polymers: Effects of Main Chain and Side Chain Lengths of Grafts. *Colloids Surf., B* **2009**, *70* (1), 53–59.

(27) Feng, W.; Zhu, S.; Ishihara, K.; Brash, J. L. Protein Resistant Surfaces: Comparison of Acrylate Graft Polymers Bearing Oligo-Ethylene Oxide and Phosphorylcholine Side Chains. *Biointerphases* **2006**, *1* (1), 50–60.

(28) Panzarasa, G.; Soliveri, G.; Sparnacci, K.; Ardizzone, S. Patterning of Polymer Brushes Made Easy Using Titanium Dioxide: Direct and Remote Photocatalytic Lithography. *Chem. Commun.* **2015**, *51* (34), 7313–7316.

(29) Hucknall, A.; Simnick, A. J.; Hill, R. T.; Chilkoti, A.; Garcia, A.; Johannes, M. S.; Clark, R. L.; Zauscher, S.; Ratner, B. D. Versatile Synthesis and Micropatterning of Nonfouling Polymer Brushes on the Wafer Scale. *Biointerphases* **2009**, *4* (2), FA50–FA57.

(30) Verduzco, R.; Li, X.; Peseck, S. L.; Stein, G. E. Structure, Function, Self-assembly, and Applications of Bottlebrush Copolymers. *Chem. Soc. Rev.* **2015**, *44* (8), 2405–2420.

(31) Ma, H.; Li, D.; Sheng, X.; Zhao, B.; Chilkoti, A. Protein-resistant Polymer Coatings on Silicon Oxide by Surface-initiated Atom Transfer Radical Polymerization. *Langmuir* **2006**, *22* (8), 3751–3756.

(32) Hucknall, A.; Kim, D. H.; Rangarajan, S.; Hill, R. T.; Reichert, W. M.; Chilkoti, A. Simple Fabrication of Antibody Microarrays on Nonfouling Polymer Brushes with Femtomolar Sensitivity for Protein Analytes in Serum and Blood. *Adv. Mater.* **2009**, *21* (19), 1968–1971.

(33) Ferris, R.; Hucknall, A.; Kwon, B. S.; Chen, T.; Chilkoti, A.; Zauscher, S. Field-Induced Nanolithography for Patterning of Non-Fouling Polymer Brush Surfaces. *Small* **2011**, *7* (21), 3032–3037.

(34) Gao, T.; Wang, X.; Yu, B.; Wei, Q.; Xia, Y.; Zhou, F. Noncovalent Microcontact Printing for Grafting Patterned Polymer Brushes on Graphene Films. *Langmuir* **2013**, *29* (4), 1054–1060.

(35) Ahmad, S. A.; Leggett, G. J.; Hucknall, A.; Chilkoti, A. Micro- and Nanostructured Poly[oligo(ethylene glycol)methacrylate] Brushes Grown from Photopatterned Halogen Initiators by Atom Transfer Radical Polymerization. *Biointerphases* **2011**, *6* (1), 8–15.

(36) Michel, R.; Pasche, S.; Textor, M.; Castner, D. G. Influence of PEG Architecture on Protein Adsorption and Conformation. *Langmuir* **2005**, *21* (26), 12327–12332.

(37) Welch, M. E.; Ritzert, N. L.; Chen, H.; Smith, N. L.; Tague, M. E.; Xu, Y.; Baird, B. A.; Abuña, H. D.; Ober, C. K. Generalized Platform for Antibody Detection using the Antibody Catalyzed Water Oxidation Pathway. *J. Am. Chem. Soc.* **2014**, *136* (5), 1879–1883.

(38) Leskela, M.; Ritala, M. Atomic Layer Deposition Chemistry: Recent Developments and Future Challenges. *Angew. Chem., Int. Ed.* **2003**, *42* (45), 5548–5554.

(39) Schindelin, J.; Arganda-Carreras, I.; Frise, E.; Kaynig, V.; Longair, M.; Pietzsch, T.; Preibisch, S.; Rueden, C.; Saalfeld, S.; Schmid, B.; Tinevez, J. Y.; White, D. J.; Hartenstein, V.; Eliceiri, K.; Tomancak, P.; Cardona, A. Fiji: An Open-source Platform for Biological-image Analysis. *Nat. Methods* **2012**, *9* (7), 676–682.

(40) Simakova, A.; Averick, S. E.; Konkolewicz, D.; Matyjaszewski, K. Aqueous ARGET ATRP. *Macromolecules* **2012**, *45* (16), 6371–6379.

(41) Matyjaszewski, K.; Xia, J. Atom Transfer Radical Polymerization. *Chem. Rev.* **2001**, *101* (9), 2921–2990.

(42) Ma, H. W.; Hyun, J. H.; Stiller, P.; Chilkoti, A. "Non-fouling" Oligo(ethylene glycol)-functionalized Polymer Brushes Synthesized by Surface-initiated Atom Transfer Radical Polymerization. *Adv. Mater.* **2004**, *16* (4), 338–341.

(43) Rotole, J. A.; Sherwood, P. M. A. Gamma-Alumina (γ -Al₂O₃) by XPS. *Surf. Sci. Spectra* **1998**, *5* (1), 18–24.

(44) Barreca, D.; Battiston, G. A.; Gerbasi, R.; Tondello, E.; Zanella, P. Zirconium Dioxide Thin Films Characterized by XPS. *Surf. Sci. Spectra* **2000**, *7* (4), 303–309.

(45) Diebold, U.; Madey, T. E. TiO₂ by XPS. *Surf. Sci. Spectra* **1996**, *4* (3), 227–231.

(46) van der Heide, P. *X-Ray Photoelectron Spectroscopy: An Introduction to Principles and Practices*; John Wiley and Sons: Hoboken, NJ, 2011.

(47) Schroder, D. K. *Semiconductor Material and Device Characterization*; John Wiley & Sons: New York, 2006.

(48) Capper, P.; Safa, K.; Koughia, C. *Springer Handbook of Electronic and Photonic Materials*; Springer: Berlin, 2006.

(49) Zhang, Z.; Zhang, M.; Chen, S.; Horbett, T. A.; Ratner, B. D.; Jiang, S. Blood Compatibility of Surfaces with Superlow Protein Adsorption. *Biomaterials* **2008**, *29* (32), 4285–4291.

(50) Chen, S.; Li, L.; Zhao, C.; Zheng, J. Surface hydration: Principles and Applications Toward Low-fouling/Nonfouling Biomaterials. *Polymer* **2010**, *51* (23), 5283–5293.

(51) Al-Hamarneh, I. F.; Pedrow, P. D.; Goheen, S. C.; Hartenstein, M. J. Impedance Spectroscopy Study of Composite Thin Films of Hydrated Polyethylene Glycol. *IEEE Trans. Plasma Sci.* **2007**, *35* (5), 1518–1526.

(52) Herrwerth, S.; Eck, W.; Reinhardt, S.; Grunze, M. Factors that Determine the Protein Resistance of Oligoether Self-assembled Monolayers - Internal Hydrophilicity, Terminal Hydrophilicity, and Lateral Packing Density. *J. Am. Chem. Soc.* **2003**, *125* (31), 9359–9366.

(53) Wang, R. Y.; Himmelhaus, M.; Fick, J.; Herrwerth, S.; Eck, W.; Grunze, M. Interaction of Self-assembled Monolayers of Oligo-(ethylene glycol)-terminated Alkanethiols with Water Studied by Vibrational Sum-frequency Generation. *J. Chem. Phys.* **2005**, *122* (16), 164702.

(54) Lutz, J. F.; Akdemir, O.; Hoth, A. Point by Point Comparison of Two Thermosensitive Polymers Exhibiting a Similar LCST: Is the Age of Poly(NIPAM) Over? *J. Am. Chem. Soc.* **2006**, *128* (40), 13046–13047.

(55) Li, L.; Chen, S.; Zheng, J.; Ratner, B. D.; Jiang, S. Protein Adsorption on Oligo(ethylene glycol)-terminated Alkanethiolate Self-assembled Monolayers: The Molecular Basis for Nonfouling Behavior. *J. Phys. Chem. B* **2005**, *109* (7), 2934–2941.

(56) Tedja, R.; Soeriyadi, A. H.; Whittaker, M. R.; Lim, M.; Marquis, C.; Boyer, C.; Davis, T. P.; Amal, R. Effect of TiO₂ Nanoparticle Surface Functionalization on Protein Adsorption, Cellular Uptake and Cytotoxicity: the Attachment of PEG Comb Polymers Using Catalytic Chain Transfer and Thiol-ene Chemistry. *Polym. Chem.* **2012**, *3* (10), 2743–2751.

(57) He, H.; Jing, W.; Xing, W.; Fan, Y. Improving Protein Resistance of α -Al₂O₃ Membranes by Modification with POEGMA Brushes. *Appl. Surf. Sci.* **2011**, *258* (3), 1038–1044.

(58) Shi, X.; Wang, Y.; Li, D.; Yuan, L.; Zhou, F.; Wang, Y.; Song, B.; Wu, Z.; Chen, H.; Brash, J. L. Cell Adhesion on a POEGMA-modified Topographical Surface. *Langmuir* **2012**, *28* (49), 17011–17018.